Kernel-Function-Based Models for Acoustic Localization of Underwater Vehicles

Breno C. Pinheiro, Ubirajara F. Moreno, João T. B. de Sousa, and Orlando C. Rodríguez

***Abstract*—This paper proposes a novel design for the localization system of autonomous underwater vehicles (AUVs) using acoustic signals. The solution presented exploits models based on kernel functions with two main purposes: 1) to reject outliers; and 2) to correct or improve accuracy of measurements. The localization system discussed is based on well-established techniques such as support vector data description (SVDD) and autoassociative kernel regression (AAKR) derived from machine learning theory that utilizes heuristic models for classification and regression tasks, respectively. By coupling the algorithm to the navigation system, we seek to reduce the sensitivity of the localization scheme to the reflected acoustic waves or fluctuations of underwater channel properties without modifying the solution used for data fusion or overloading the algorithm embedded in the vehicle. Data collected in the field with a light underwater vehicle (LAUV) were used to demonstrate the advantages of the proposed approach.**

***Index Terms*—Acoustic localization, underwater vehicles, statistical learning theory, kernel-based models.**

I. Introduction

OVER the past few years, interest in underwater vehicles for applications in security, rescue, archaeological research, etc., has grown significantly. In environmental monitoring, for instance, these platforms have become fundamental tools for gathering data from aquatic ecosystems [1], for taking pictures of the environment's geography, and also for inspecting underwater structures [2]. Technological advances have made autonomous underwater vehicles (AUVs) suitable to support missions covering large areas and, because they are equipped with off-the-shelf sensors, capable of measuring chemical and biological variables in dynamic environments, such as oceans and rivers [3]–[5].

Despite the high technological advance in inertial sensors, which provide accurate information about motion and orientation, the acoustic localization system remains critical for improving the accuracy of navigation. The field of underwater acoustic localization can be investigated from different perspectives. One of them relates to the configuration of acoustic sensors that can be fixed at known positions in the environment, such as in buoys equipped with global positioning system (GPS) [6] or installed in other vehicles in a cooperative configuration [7]. Regarding the mitigation of uncertainties associated with underwater sensing, there are solutions for data fusion using Bayesian filters (e.g., extended Kalman filter (EKF) [8]), and using numerous nonparametric approaches (e.g., work of Caiti *et al.* [9]) through the set-membership formulation or using numerical methods such as the particle filter in [10].

This study proposes a design for the acoustic localization, considering the most widely used scheme for this purpose, the long baseline (LBL) [11] , [12]. In this configuration, an AUV transceiver pings several transponders, which have been deployed in known locations, and listens for sequential replies. The time of flight (ToF) of these waves carries information about the relative position of the vehicle. Here, the solution presented enhances the acoustic localization performance usually degraded by high noise levels, multiple wave reflections, and significant changes in the sound-speed profile throughout the water column. The main idea of the algorithm is the use of measurement history through empirical models for two main purposes: 1) to reject outliers; and 2) to correct or improve the accuracy of the ToF measurement. The latter one deals with the raw data, while the former one looks for a standard behavior in the residuals generated.

Recently, the process of learning from data has been used in applications related to signal processing. For acoustic localization, we observe the study carried out in [13] where the bias in a semicoherent ToF estimation is corrected using a regression model. The model outputs an additive offset, which is used to correct the misidentification of the main peak in the matched filter. Interesting results are achieved in [14]–[16] using a pattern matching algorithm to treat the underwater localization. In this case, the goal is to predict the receiver location from an acoustic-signal map. The probability that a received signal occurred at an arbitrary location is viewed as the weight for reference location selected at the online stage. Statistical learning theory [17], particularly the support vector machines (SVMs), was employed in [18] to reduce the influence of the change of statistical properties in the system noise and the observed noise in a simultaneous localization and mapping framework for vehicle localization. In relation to antenna array processing and electromagnetic application, the use of SVM is also discussed in [19] and [20] for issues such as beamforming and determining of the angle of arrival. In previous studies [21], the authors have exploited the kernel-based framework to correct deviations in the ToF measurements. The experimental results showed that a significant number of measurements rejected by the outlier rejection scheme running in the vehicle could be corrected and utilized by the state estimation filter in the same mission.

Manuscript received November 27, 2014; revised November 15, 2015 and March 29, 2016; accepted June 2, 2016.

Associate Editor: J. Gomes.

B. C. Pinheiro and U. F. Moreno are with the Department of Automation and System, Federal University of Santa Catarina, Florianópolis, Santa Catarina 88040-900, Brazil (e-mail: breno.pinheiro@posgrad.ufsc.br; ubirajara.f.moreno@ufsc.br).

J. T. B. de Sousa is with the Underwater Systems and Technologies Laboratory (USTL), Faculty of Engineering, University of Porto, Porto, Portugal (e-mail: jtasso@fe.up.pt).

O. C. Rodríguez is with LARSyS, Algarve University, Faro, Portugal (e-mail: orodrig@ualg.pt).

Digital Object Identifier 10.1109/JOE.2016.2578218

The novelty of this paper is the integration of empirical models in the navigation system not only to improve accuracy as discussed in our previous work, but also to identify outliers in the ToF measurements, which are strongly related to localization of AUVs. To this end, the approach here makes use of kernel-function-based models constructed either offline or online with recent measurements and residuals previously accepted by a rejection scheme. These models are continuously updated and used during navigation to correct or improve the accuracy of subsequent measurements. We confirm the effectiveness of the integrated navigation system with the experimental data where exogenous sources of error were inserted to evaluate the gain obtained with the new algorithm.

We organized this paper as follows. Section II shows the proposed design describing each block functionality and pointing out some relevant characteristics regarding the navigation system. Section III brings up the algorithm and procedures used to process the information from acoustic sensing. Section IV carries out an analysis with respect to model formulation, along with methods for adjusting the parameters, while Section V brings some numerical results using real data and the adopted sound wave propagation model. In Section VI, some alternatives that are to be exploited afterwards and limitations are also discussed. Section VII is the concluding section where some future studies are presented.

II. Navigation System

A. Proposed Design

The navigation system involves determining the position, velocity, and orientation of a rigid body relative to some coordinate system [22]. It usually uses the inertial properties of the sensors embedded in the vehicle to perform navigation functions by processing the data from the inertial sensors, which provides information regarding acceleration and angular displacement. The inertial navigation system (INS) works in the integration of these quantities to determine the position, velocity, and orientation of the vehicle [23].

In a scenario where measurements are very noisy, the notion of aided navigation is fundamental, as it refers to the process of merging data from the sensors attached to the vehicle that perform readings of some quantities related to its states. The architecture for the navigation system analyzed in this work is detailed in Fig. 1, where the state estimation is performed by a multirate EKF that propagates and updates the error covariance along with the system states whenever external measurements are available. In the figure, the states of the system states are the vectors p, v, and λ, which represents the position, velocity, and orientation of the vehicle, respectively.

As depicted in Fig. 1, this study focuses on classifying and improving the accuracy of the measured sound waves' ToFs in the acoustic localization system. The figure shows that the solution proposed is decoupled from the state estimation filter, specifically acting in ToF measurements. Thus, whenever a vector of measurements (z_{k+1}^{-}) deriving from acoustic emitters is available, it begins the process of classifying and correcting of these measurements. The whole process is based on four fundamentals steps:

Step 1) residuals generation with measured ToFs;
Step 2) residuals analysis with measured ToFs;
Step 3) correction of the measured ToFs;
Step 4) residuals analysis with corrected ToFs.

In our approach, the residuals are first generated using the measured ToFs (z_{k+1}^{-}) and the estimated quantities $(\hat{z}_{k+1})$, which are calculated using a model of the ToF that takes into account the estimated vehicle position (p_{k+1}^{-}). In the subsequent step, inside the residual analysis block, we aim to obtain information on how well the generated residual is represented by the database that was previously established to set the correction algorithm properly. In this study, such relation is achieved by using a data description model that concentrates good samples from the database inside a boundary region.

The next step is the correction, which is carried out inside the correction and analysis block, where an autoassociative regression model is used to raise the accuracy of the measured ToF using a database composed by corrected examples of time of propagation previously gathered in the navigation area. It should be emphasized that those examples are the same as those utilized to provide the residuals that compose the database for data description. Through the usage of kernel functions, it is possible to control the generalization capabilities of the regression model taking into account some statistic of the stored data provided by the stated residual analysis.

In the last step, the residual generated using the new ToF is analyzed again by the same data description model to classify the corrected ToF either as an accepted or as an outlier measurement. The following sections discuss details about the mentioned steps, including the adopted strategies.

B. Extended Kalman Filter

The EKF is the fundamental algorithm used for the data fusion process to dynamically compensate for the effects of noise and bias usually present in inertial sensors. The system state vector

$$x = [p^T \quad v^T \quad \lambda^T \quad b_{\mathrm{ac}}^T \quad b_{\omega}^T]^T$$

is composed of the vehicle's position $p \in \mathbb{R}^3$ and speed $v \in \mathbb{R}^3$, both in the local reference frame (north–east–down); the rotational vector $\lambda \in \mathbb{R}^3$; and the three-axis random walk bias values b_{ac}, $b_{\omega} \in \mathbb{R}^3$ from accelerometer (ac), and gyroscope (ω) readings, respectively. The notation ^{T} corresponds to the transpose operator. However, the filter formulation used in this work involves an error state–space model, where the measured residuals are computed from the system's output that are composed by inertial sensors/INS and the output of aid sensors. The error state vector is

$$\delta x = \left[\delta p^T \quad \delta v^T \quad \delta \lambda^T \quad \delta b_{\mathrm{ac}}^T \quad \delta b_{\omega}^T\right]^T.$$

In [8], [24], and [25], the formulation using such a model is properly discussed and uses the following state–space representation of the dynamic system:

$$\begin{aligned}
\delta \dot{p} &= \delta v \\
\delta \dot{v} &= -C_B^N \delta b_{\mathrm{ac}} - [C_B^N \, {}^b a_{\mathrm{sf}} \times] \delta \lambda + C_B^N \, n_{\mathrm{ac}} \\
\delta \dot{\lambda} &= -C_B^N \delta b_{\omega} + C_B^N \, n_{\omega} \\
\delta \dot{b}_{\mathrm{ac}} &= -n_{b_{\mathrm{ac}}} \\
\delta \dot{b}_{\omega} &= -n_{b_{\omega}}
\end{aligned} \tag{1}$$

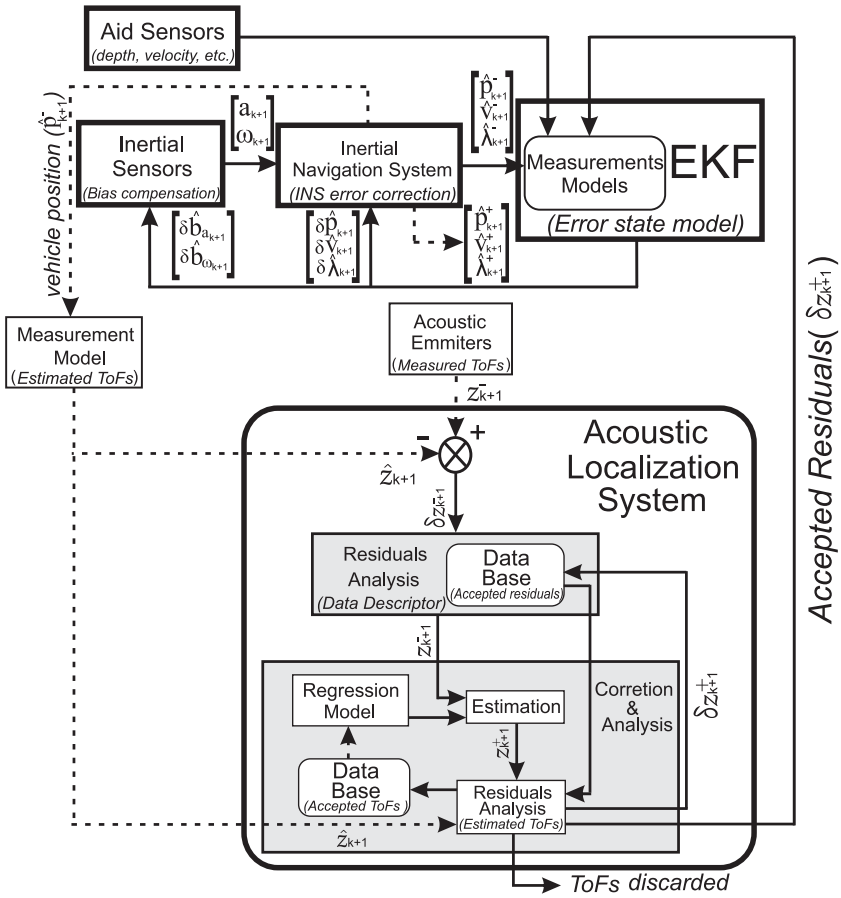

Fig. 1. Block diagram of the proposed navigation system. The acoustic localization estimation block acts exclusively in the ToFs measurements with no changes in the navigation algorithm.

where δ indicates the difference between the actual state and its estimated value, ${}^{b}a_{\mathrm{sf}}$ is acceleration due some specific forces (sf) in body (b) reference frame, $[\cdot\times]$ refers to the skew-symmetric matrix, and $\delta\boldsymbol{\lambda}$ is the error of orientation. The values δb_{ac} and δb_{ω} represent the bias compensation error in the accelerometer and gyro outputs, respectively. The matrix $C_B^N \in SO(3)$ is a direction cosine matrix, parameterized by the vector of rotation angles about three orthogonal axes in body-fixed frame $(\mathbf{B})$ (roll, pitch, yaw)

$$\boldsymbol{\lambda} = [\phi \quad \theta \quad \psi]^T$$

and referring to a rotation matrix from body to local reference frame $(\mathbf{N})$. The input vector of additive noise n inserted in the process model to represent the uncertainties in the prediction stage is

$$n = \begin{bmatrix} n_{\mathrm{ac}}^T & n_{\omega}^T & n_{b_{\mathrm{ac}}}^T & n_{b_{\omega}}^T \end{bmatrix}^T, \quad n \sim N(0, Q(t))$$

where all quantities are modeled as zero-mean, white, and uncorrelated Gaussian process with error variance matrix $Q(t)$. The resulting continuous-time error state system is

$$\delta\dot{x} = F(t)\delta x(t) + G(t)u(t). \tag{2}$$

Matrices $F(t)$ and $G(t)$ are defined according to

$$F(t) = \begin{bmatrix} 0_{3\times3} & \mathrm{I}_{3\times3} & 0_{3\times3} & 0_{3\times3} & 0_{3\times3} \\ 0_{3\times3} & 0_{3\times3} & -\left[C_B^N\ {}^{b}a_{\mathrm{sf}}\times\right] & -C_B^N & 0_{3\times3} \\ 0_{3\times3} & 0_{3\times3} & 0_{3\times3} & 0_{3\times3} & -C_B^N \\ 0_{3\times3} & 0_{3\times3} & 0_{3\times3} & 0_{3\times3} & 0_{3\times3} \\ 0_{3\times3} & 0_{3\times3} & 0_{3\times3} & 0_{3\times3} & 0_{3\times3} \end{bmatrix} \tag{3}$$

$$G(t) = \begin{bmatrix} 0_{3\times3} & 0_{3\times3} & 0_{3\times3} & 0_{3\times3} \\ C_B^N & 0_{3\times3} & 0_{3\times3} & 0_{3\times3} \\ 0_{3\times3} & C_B^N & 0_{3\times3} & 0_{3\times3} \\ 0_{3\times3} & 0_{3\times3} & -\mathrm{I}_{3\times3} & 0_{3\times3} \\ 0_{3\times3} & 0_{3\times3} & 0_{3\times3} & -\mathrm{I}_{3\times3} \end{bmatrix} \tag{4}$$

where I is the identity matrix.

An equivalent discrete-time model is used to propagate the navigation state, the error state, and the covariance matrix of an estimation error through time. The error state δx_k^+ and the covariance matrix of estimation error P_k^+ are propagated from time k to $k+1$, corresponding to the integration period Δt from

the INS by using the transition matrix Φ_k according to

$$\delta x_{k+1}^{-} = \Phi_k \delta x_k^{+} \tag{5}$$

$$P_{k+1}^{-} = \Phi_k \; P_k^{+} \; \Phi_k^T + \Gamma_k \; Q_k \; \Gamma_k^T \tag{6}$$

where the superscripts $^-$ and $^+$ indicate the *a priori* and the *a posteriori* state estimation. The transition matrices Φ_k and $\Gamma_k Q_k \Gamma_k^T$ are given as

$$\Phi_k = \exp(E \; \Delta t) \tag{7}$$

$$\Gamma_k \; Q_k \; \Gamma_k^T = G \; Q \; G^T \Delta t \tag{8}$$

where the time-varying system matrix E in (7) is the Jacobian matrix derived from the differential equation (2) evaluated with the current state x_k^+ , and the exponential can be computed using algorithms from [26]. The expected value of the state δx_k from k to $k+1$ is zero, which represents the best *a priori* estimation of the error state until a new measurement z_k becomes available. Then, both the error state and the covariance matrix are updated using the following procedure:

$$K_{k+1} = P_{k+1}^{-} H_{k+1}^T \left(H_{k+1} P_{k+1} - H_{k+1}^T + \Upsilon_{k+1} \right)^{-1} \tag{9}$$

$$\delta x_{k+1}^{+} = \delta x_{k+1}^{-} + K_{k+1} \left(\delta z_{k+1} - H_{k+1} \delta x_{k+1}^{-} \right) \tag{10}$$

$$P_{k+1}^{+} = (I - K_{k+1} H_{k+1}) P_{k+1}^{-} \tag{11}$$

where K_{k+1} is the Kalman gain, H_{k+1} is the partial derivative matrix of the sensor output evaluated at the current state estimate, and Υ_{k+1} represents the covariance matrix of the measurement noise. The variable δz_{k+1} in (10) represents the residual between the measurement model and the corresponding measurement from the sensor. Whenever δx_{k+1}^{+} is calculated, the previous output $\hat{x}_{k+1}^{-} = [\hat{p}_{k+1}^{-}, \hat{v}_{k+1}^{-}, \hat{\lambda}_{k+1}^{-}, \hat{b}_{a\,k+1}^{-}, \hat{b}_{\omega\,k+1}^{-}]^T$ from the inertial sensors/INS block regarding the vehicle state and the bias value is updated using

$$\hat{x}_{k+1}^{+} = \hat{x}_{k+1}^{-} + \delta x_{k+1}^{+}$$

and the corresponding error state δx_{k+1}^{+} returns to zero in the next iteration [8]. In accordance with [25] and [23], the rotation matrix C_{k+1}^{-}, where $C \equiv C_B^N$ was used to simplify the notation, is compensated for by using the rotation error matrix $C_{k+1}^T(\delta\hat{\lambda}_{k+1})$ parameterized by the vector $\delta\lambda_{k+1}$ according to

$$C_{k+1}^{+} = C_{k+1}^T(\delta\hat{\lambda}_{k+1}) \; C_{k+1}^{-}. \tag{12}$$

The rotation error matrix is computed by

$$C_{k+1}(\delta\hat{\lambda}_{k+1}) = \; I_{3\times 3} + \frac{\sin \parallel \delta\hat{\lambda}_{k+1} \parallel}{\parallel \delta\hat{\lambda}_{k+1} \parallel} [\delta\hat{\lambda}_{k+1}\times] + \frac{1 - \cos \parallel \delta\hat{\lambda}_{k+1} \parallel}{\parallel \delta\hat{\lambda}_{k+1} \parallel^2} \tag{13}$$

where $\| \cdot \|$ represents the Euclidean norm. Equations (12) and (13) confirm that it is a nonlinear system since matrix C_{k+1}^{+} is a function of the state $\delta\hat{\lambda}_{k+1}$.

The advantage of the state estimation process presented in this section is its decoupling from the model of the underwater vehicle and its particular emphasis on the propagation of residuals described by the state variables δx. However, our approach focuses on the generation of the residual δz_{k+1} by considering ToFs measurements. The residual is first analyzed on the basis of how well it is described by the residual database. The result is used to assist in the tuning of the regression function in the correction routine. After correction, a new residual is generated and reanalyzed by the same data descriptor to qualify the current ToF as either a valid or an outlier measurement.

C. Generation of Residuals

Consider $z_k^- \in \mathbb{R}^{n\times 1}$ as the ToFs' measurement vector from n transponders before correction and z_k^+ the same vector after the correction procedure. The expression $\hat{z}_k = h(\hat{x}_k^-)$ is an estimation of such a quantity using the measurement model as follows:

$$\hat{z}_k[i,j] = \frac{1}{c(t_0)} \| B_j - p(t_0) \| + \frac{1}{c(t_k)} \| B_j - p(t_k) \| \tag{14}$$

where $c(t)$ corresponds to the speed of sound in water at time t, B_j is the position of the transponder j, and $p(t)$ is the transceiver's position installed in the vehicle. The instants t_0 and t_k refer to the time stamp of interrogation and receipt of reply, respectively. It is worth noting that when a sequential scheme for LBL acoustic localization is used, each transponder waits for a period of time T_j before replying to the interrogation. In this case, such a quantity must be added to the measurement model (14) for each transponder.

In the subsequent analysis, the vector of ToF residuals δz_k is calculated using the measurement model $\hat{z}_k$ and the actual measurement before z_k^- and after z_k^+ correction:

$\delta z_k^- = z_k^- - \hat{z}_k$: residuals calculated from incoming ToF measurements;

$\delta z_k^+ = z_k^+ - \hat{z}_k$: residuals calculated from corrected ToF measurements.

Such a variable is supposed to bring innovation to the data fusion process performed by the EKF. However, due to the numerous sources of errors, such as changes in the sound-speed profile [27], external noise, and multipath reflection at the wave guide [28]–[30] that are inherent to the underwater acoustic communication, further analysis of the reliability of that information is required.

To provide information about the quality of the measured ToFs, our design proposes an investigation regarding the similarities between δz_k and a database of residuals generated previously in the same area of navigation. For this purpose, the machine learning theory was exploited to get a description of the examples in the database and to classify the generated residual.

D. Analysis of Residuals

As already introduced, the empirical model constructed from residuals aims to identify some statistic of the data from acoustic localization and use that description to qualify subsequent measurements as carrying accepted or rejected information.

The strategy adopted here uses a support vector classifier proposed by Tax in [31] and [32] known as support vector data description (SVDD), whose theoretical foundations lay on statistical learning theory [33], [34]. This method is designed to give a description of a set of objects and can be used for novelty or outlier detection [35]. The SVDD is also suitable for one-class classification tasks, when one of the classes is well sampled while the other is not. The data description is used here for purposes of the analysis of residuals δz_k and to work in conjunction with EKF, which updates the vehicle states continuously.

So, the method aims to obtain a spherically shaped boundary around the target set to describe it. In our case, the target set contains $m \times n$ vectors of residuals from accepted measurements obtained before or even during navigation, where m is the total number of training objects and n is the number of transponders.

1) Theory Formulation: This part of the work is dedicated to the presentation of a brief overview of the SVDD theory by Tax. The mentioned boundary around the data set is completely defined by the center $a \in \mathbb{R}^n$ of the hypersphere and the radius $R \in \mathbb{R}$ where $R > 0$. First, an error function L is defined to be minimized

$$L(R, a) = R^2$$

with the constraints

$$\| \delta z_i - a \|^2 \leq R^2 \quad \forall i.$$

By minimizing R^2, the method gives a closed boundary containing all training objects δz_i , $i = 1, \ldots, m$. To make the solution more robust allowing outliers, namely examples whose distance to the center is larger than the radius, in the training set, a slack variable $\xi \geq 0$ is inserted, but large values are penalized by parameter Ω. Function L is rewritten as

$$L(R, a) = R^2 + \Omega \sum_i \xi_i \tag{15}$$

with the constraints

$$\| \delta z_i - a \|^2 \leq R^2 + \xi_i, \quad \xi_i \geq 0 \quad \forall i. \tag{16}$$

The minimization process is simplified by incorporating constraints (16) in (15) through Lagrange multipliers $\alpha_i \geq 0, \gamma_i \geq 0$

$$\begin{aligned} L(R, a, \alpha_i, \gamma_i, \xi_i) &= R^2 + \Omega \sum_i \xi_i \\ &- \sum_i \alpha_i \left\{ R^2 + \xi i - (\| \delta z_i \|^2 - 2a \cdot \delta z_i + \| a \|^2) \right\} \\ &- \sum_i \gamma_i \xi_i. \end{aligned} \tag{17}$$

In (17), L is minimized with respect to R, a, and ξ_i and maximized with respect to α_i and γ_i. By setting partial derivatives of L with respect to R, a, and ξ_i to zero, the resulting constraints are, respectively

$$\sum_i \alpha_i = 1 \tag{18}$$

$$a = \frac{\sum_i \alpha_i \delta z_i}{\sum_i \alpha_i} \tag{19}$$

$$\Omega - \alpha_i - \gamma_i = 0. \tag{20}$$

Using (19), the center a of the hypersphere can be calculated, while (20) results in $0 \leq \alpha_i \leq \Omega$, where Ω becomes an upper boundary for Lagrange multipliers α_i. Resubstituting (18)–(20) into (17) leads to solving the dual problem

$$L = \sum_i \alpha_i (\delta z_i \cdot \delta z_i) - \sum_{i,j} \alpha_i, \alpha_j (\delta z_i \cdot \delta z_j) \tag{21}$$

with the constraints

$$0 \leq \alpha_i \leq \Omega. \tag{22}$$

Maximizing (21) gives a set α_i where

$$\| \delta z_i - a \|^2 < R^2 \rightarrow \alpha_i = 0, \qquad \gamma_i = 0 \tag{23}$$

$$\| \delta z_i - a \|^2 = R^2 \rightarrow 0 \leq \alpha_i \leq \Omega, \qquad \gamma_i = 0 \tag{24}$$

$$\| \delta z_i - a \|^2 > R^2 \rightarrow \alpha_i = \Omega, \qquad \gamma_i > 0. \tag{25}$$

Those examples with $\alpha_i > 0$ are chosen for data description and are referred to as support vectors (SVs). To test a general object δz_k regarding its acceptance in the data set, the distance to the center a of the hypersphere has to be calculated using

$$\begin{aligned} \| \delta z_k - a \|^2 \; &= \; (\delta z_k \cdot \delta z_k) - 2 \sum_i \alpha_i (\delta z_k \cdot \delta z_i) \\ &+ \sum_{i,j} \alpha_i \alpha_j (\delta z_i \cdot \delta z_j) \leq R^2. \end{aligned} \tag{26}$$

Examples with distances smaller than the radius are accepted or classified as belonging to the target class. On the other hand, SVs with $\alpha_i = \Omega$ are classified as outliers and fall outside the hypersphere. Those that have $0 < \alpha_i < \Omega$, henceforth identified as δz_{sv}, are used to calculate the radius of the hypersphere because they are on the boundary. Then

$$\begin{aligned} R^2 \; &= \; (\delta z_{\mathrm{sv}} \cdot \delta z_{\mathrm{sv}}) - 2 \sum_i \alpha_i (\delta z_i \cdot \delta z_{\mathrm{sv}}) \\ &+ \sum_{i,j} \alpha_i \alpha_j (\delta z_i \cdot \delta z_j). \end{aligned} \tag{27}$$

In (21), (26), and (27), the inner product $(\delta z_i \cdot \delta z_j)$ can be replaced by kernel functions to obtain more flexible solutions [32], [34]. By using kernel functions, it is possible to have a similar measure corresponding to an inner product in a so-called higher dimensional feature space where the data characteristics are more distinguishable [36].

For improvements in data description, negative examples identified as belonging to an outlier class can be incorporated into the training set to get a better description of the target data set. Besides this, when some outliers are expected in the training set $(m \times n)$, the value of Ω can be defined as $\Omega \leq (1/(n \cdot (\mathrm{fraction\ outlier})))$, which gives more flexibility to the sample acceptance criterion that is an essential idea when the database is continuously updated.

With the preceding formulation, the ToF measurements that generate residuals inside the hypersphere are classified as accepted, while the others are rejected. From this analysis, it is also possible to conclude the level of acceptance or rejection made by calculating the distance of the residual to the center of the hypersphere using (26).

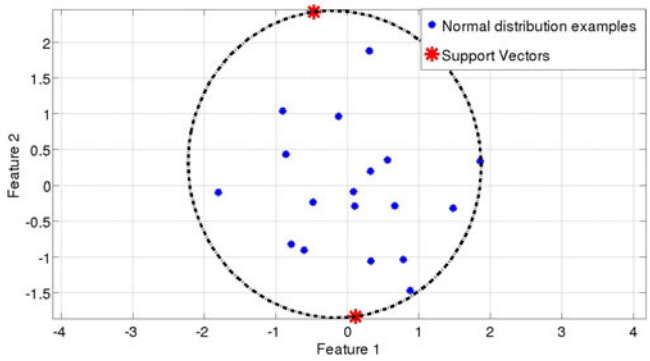

Fig. 2. Example of data description. Kernel is a Gaussian function with width $s = 5$ and $\Omega = 1$.

2) Example 1: As a simple example, we investigate a 2-D synthetic data $x_{i,j}$ drawn from a normal distribution with zero mean ($\mu = 0$) and unit standard deviation ($\sigma = 1$). For the data description algorithm, we used a very intuitive tool [37] along with a Gaussian kernel according to

$$K(x_i, x_j) = \exp(\|x_i - x_j\|/s^2)$$

where parameter s, in combination with Ω, controls the volume of the hypersphere and the number of SVs. As discussed in [32] and [36], for small values of the kernel width s, $K(x_i, x_j) = \exp((\|x_i - x_j\|)/s^2) \simeq 0 \ \ \forall i \neq j$, and L in (21) will be optimized when all N objects become SVs with equal $\alpha_i = (1/N)$. In this case, the solution is identical to the Parzen density estimation [38]. For larger values of s, the solution approximates a spherically shaped solution as shown in Fig. 2 where a perfectly circular boundary region was achieved with $s = 5$ and $\Omega = 1$. All SVs that fully describe the whole data set are highlighted.

3) Example 2: The next example's purpose is to investigate the mentioned influence of the choice of parameters s and Ω in the shape of the data descriptor boundary region. Here, the training process was carried out using two 2-D data sets: $\mathcal{A}_{100\times2}$ with $\mu = 0$ and $\sigma = 0.2$ defined as the target class and $\mathcal{B}_{20\times2}$ with $\mu = 0$ and $\sigma = 0.5$ defined as the outlier class, both drawn from a normal distribution. Fig. 3 shows the results for choices when $s = 5,\ 0.5$ and $\Omega = 1,\ 0.1$. As was claimed before, we see that with decreasing the parameter s, the number of SVs increased, while the choice of $\Omega = 1$ forced all target examples to be accepted. It is worth noting that the choice of $s = 0.5$ resulted in a border closer to the target objects, followed by the exclusion of some outliers. For the intermediate values of s, a weighted Parzen density estimation is obtained, where both weights of the kernel as well as the choice of the SVs are obtained by the optimization procedure.

When some outliers are expected in the target data set, parameter Ω is decreased, which constrains the values for α_i in accordance with (18) and (22). In this case, more objects are expected to become SVs, as shown in the case where $s = 5$ and $\Omega = 0.1$. As the target examples are more concentrated, a data descriptor with a smaller boundary is suggested, where some accepted examples that are less represented in the data set might be excluded. This was accomplished by using $s = 0.5,\ \Omega = 0.1$ which showed a better fit for the data set by isolating more related data and excluding some objects from the target class with fewer SVs to the data description. In all cases, if the analyzed sample is further from the center of the hypersphere, it will be represented less by the target class. It is reasonable to think that the algorithm has low extrapolation capacity as it calculates a weighted average of all the values observed. In the extreme case where there is no similarity between the stored data and the input vector, a simple average is calculated which is still a poor estimate of the real value. This result will impact how the correction will be performed in the next step.

E. Correction

The correction step is intended to improve the accuracy of the ToF measurements obtained from the acoustic system. Deviations in the measurement due to multipaths, low signal-to-noise ratio (SNR), or changes in sound-speed profile through the water column can be corrected by using the autoassociative models, where the input and output spaces are the same.

The strategy adopted in this step make use of the autoassociative kernel regression (AAKR) [39], which is a type of model based on similarities or a nonparameterized modeling technique that seeks to exploit similarities between an input vector and training data stored in memory to increase the accuracy of the sensors. The theoretical basis of the AAKR refers to the concept of general regression neural networks [40] and has been used mainly in online sensor monitoring [41].

The idea is to estimate an output vector based on the weighted sum of the training data, given an input vector. The parameter of relevance can be measured using metrics, such as distance u (e.g., Euclidean distance u^E) between the input vector of ToF z_k^- and each vector of the training data stored in a matrix $Z_{m\times n}$ with m and n as defined earlier. The technique's mathematical formulation is presented in (28). Let u_i^S be

$$u_i^S(Z_{i\times n}, z_k^-) = \sqrt{(z_k^- - z_i)^T\, S^{-1}\, (z_k^- - z_i)} \qquad (28)$$

where $i \in \{1, \ldots, m\}$, z_i^T is an $n \times 1$ vector with observations from $Z_{i\times n}$, and $S = cov(Z)$ is the covariance matrix of the data stored in Z. In the case of $S = I$ (the identity matrix), $u^S = u^E$, otherwise S can be used to make the estimation process less sensitive to any input data stored in the matrix.

The values are translated into similarities, expressed by $\mathrm{w}_{m\times1} = [w_1, \ldots, w_m]^T$, through the kernel functions such as the Gaussian function, according to

$$w_i = \frac{1}{\sqrt{2\pi h^2}} \exp\left(-\frac{u_i^2}{h^2}\right) \qquad (29)$$

where h corresponds to the kernel width. The processed output vector of ToF z_k^+ is obtained through

$$z_k^+ = \overline{\mathrm{w}}^T\, Z \quad \text{with} \quad \overline{\mathrm{w}} = \mathrm{w}/\|\mathrm{w}\|_1. \qquad (30)$$

Expression (30) states that estimate z_k^+ is a weighted average of all observed values. It is worthwhile to observe that very small values of h imply higher weights only when u_i in (29) is very close to zero. Conversely, when it is made very large, z_k^+ approximates the sample mean of the observed values. Thus, the value of h reflects a compromise between accuracy and generalization capability of the model based on kernel functions and

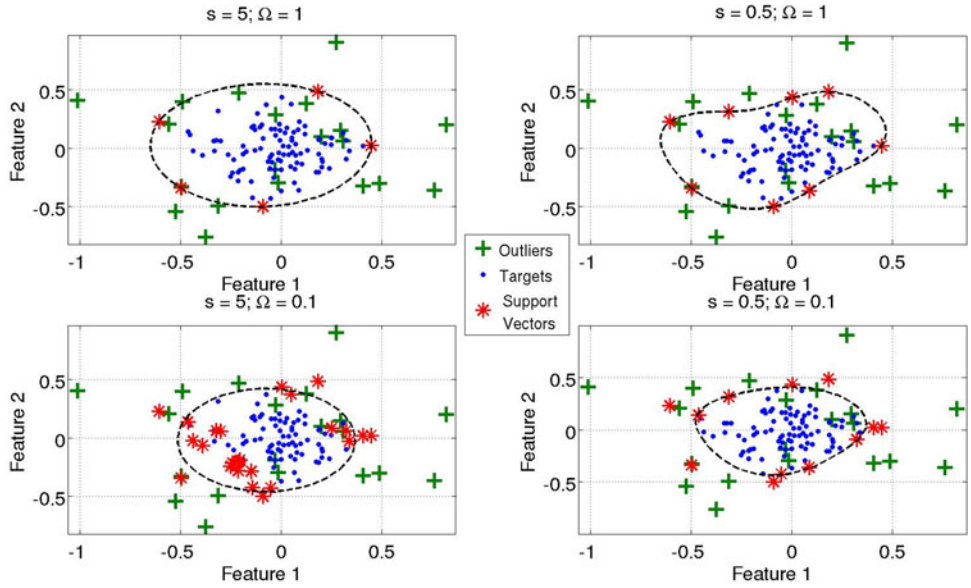

Fig. 3. Data descriptions trained on a normal distribution data set. Kernel is a Gaussian function with different widths $s = 5$, 0.5, and $\Omega = 1, 0.1$.

has to be optimized. Finally, once $\delta z_k^+ = z_k^+ - \hat{z}_k$ is accepted by the residual analysis block, it is sent to EKF; in all other cases, it is rejected, as shown in Fig. 1.

1) Cross Validation: The leave-one-out (LOO) cross-validation algorithm is a useful strategy to assess the performance of a learning algorithm on a data set [42]. In our case, the LOO analysis is used to make a better selection of the kernel bandwidth. So, by using the m samples in the data set, at each iteration, the algorithm takes one different sample z_i as a validation set, leaves $Z_{(m-1)\times n}$ samples as a learning set, and calculates the mean square error e between the real value z_i and the regression output z_k^+ according to

$$e_i = \frac{1}{n}\left[z_k^+ - z_i\right]\left[z_k^+ - z_i\right]^T, \quad \text{for } i = 1, \ldots, m$$

where z_k^+ is the estimation of z_i by taking it as unseen in the learning set. At the end, the best h is the one that gives the smaller root mean squared error (RMSE) after all $z_i \in Z$ have been used as a validation set

$$h(Z) = \arg\min_h \sqrt{\left(\frac{1}{m}\sum_{i=1}^{m} e_i\right)}.$$

2) Example: In the sequence, we discuss an example in the context of our work to show how the AAKR can improve the accuracy of the ToF measurements based on historical data. For this analysis, we use a hypothetical navigation area with four acoustic beacons deployed to locate the AUV, as shown in Fig. 4. The acoustic beacons are $l = 200$ m apart from each other.

For the composition of the training data set, circular trajectories with different radii $r = 50$, 100, 150, and 200 m in the xy-plane were used. In this case, a time matrix $Z_{750\times4}$ was constructed with ToFs calculated within the delimited area when one of the four beacons was in the center of the trajectory. Then, the training data set is a matrix $Z_{3000\times4}$ of ideal ToFs. These good samples ware used by AAKR to correct ToFs measurements from acoustic beacon 1 at a distance 50–150 m from it

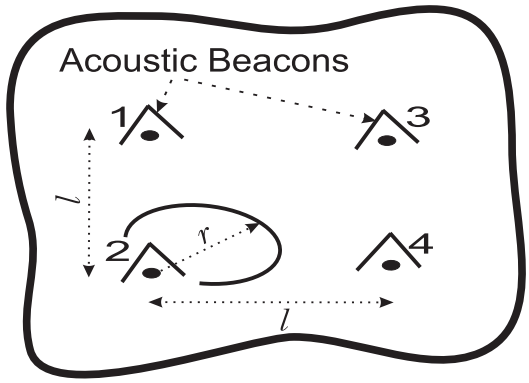

Fig. 4. LBL deployment in a hypothetical area.

and at different positions within the delimited area with a sound speed of 1500 m/s. The faulty measurements were obtained with an artificial linearly increasing drift ending at a magnitude of 0.1 s inserted in ToFs and introduced in the testing data set.

So, in this case, the AAKR has the following input and output data:

$$\text{Input} = \left[z_{t_1}^-, z_{t_2}, z_{t_3}, z_{t_4}\right]$$
$$\text{Output} = z_{t_1}^+$$

where the quantities $z_{t_{2,3,4}}$ are ToFs measurements without deviation from the corresponding beacon and $z_{t_1}^-$ is the deviated measurement to be corrected. Again, the superscripts $^-$ and $^+$ indicate the quantity prior and posterior to correction by the AAKR. Fig. 5 shows the results for 1000 ToF measurements, where it can be seen that the most significant deviations were attenuated. Regarding the kernel function (29), the bandwidth $h = 0.5$ was chosen for simplicity.

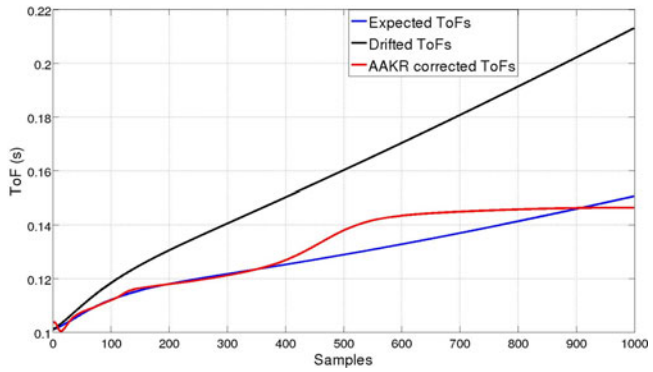

Fig. 5. Linear deviation in ToFs measurements and the corresponding correction using AAKR.

III. The Algorithm

The discussion about the algorithm begins with the flowchart shown in Fig. 6, which seeks to enlighten the whole process of the analysis of residuals and a correction of measurements.

As expected, the algorithm starts whenever a new vector of ToFs is available, with which the residual δz_k^- is calculated. Considering a data set with target residuals from past measurements and a boundary region with center a and radius R defined in advance, it is possible to evaluate the distance of the current residual to the center of the hypersphere and then compare it with the radius R using (26).

The algorithm proceeds to perform the correction of any deviations in ToFs through AAKR. For this task, the autoassociative model uses a history of the ToF measurements available in the data set. The kernel width h in (29) can be chosen taking into account the previous result from the analysis of residuals, where for accepted measurements we use h_1 while h_2 is used for rejected measurements, and $h_2 > h_1$. For accepted measurements, a smaller value of h is expected since it is very likely that a similar measurement is in the database. In this case, a heavier weight should be assigned to observations closer to the query vector. However, for rejected ones, the kernel width can be increased to enhance the generalization capacity of the regression function [40].

After correction, the posterior residuals δz_k^+ are calculated using the measurements corrected in z_k^+ and then reanalyzed by the data descriptor to confirm or to not confirm the improvements in the estimated ToFs. It might be noted that the distance to the center can be evaluated using any dimension of the input vector, which avoids discarding the entire vector of residuals, and consequently, the ToFs. In the extreme case, for instance, the residuals are taken and analyzed individually to identify the best estimate before sending to EKF. However, in our analysis, only the full vectors of accepted measurements and residuals are used to update the data sets. It should be emphasized that a new boundary region must be found whenever a new residual is incorporated into the data set.

IV. Tuning of the Acoustic Localization System

This section discusses the process of adjusting the parameters of the algorithm presented in Section III based on experiments performed in the field. The proposed design has been evaluated

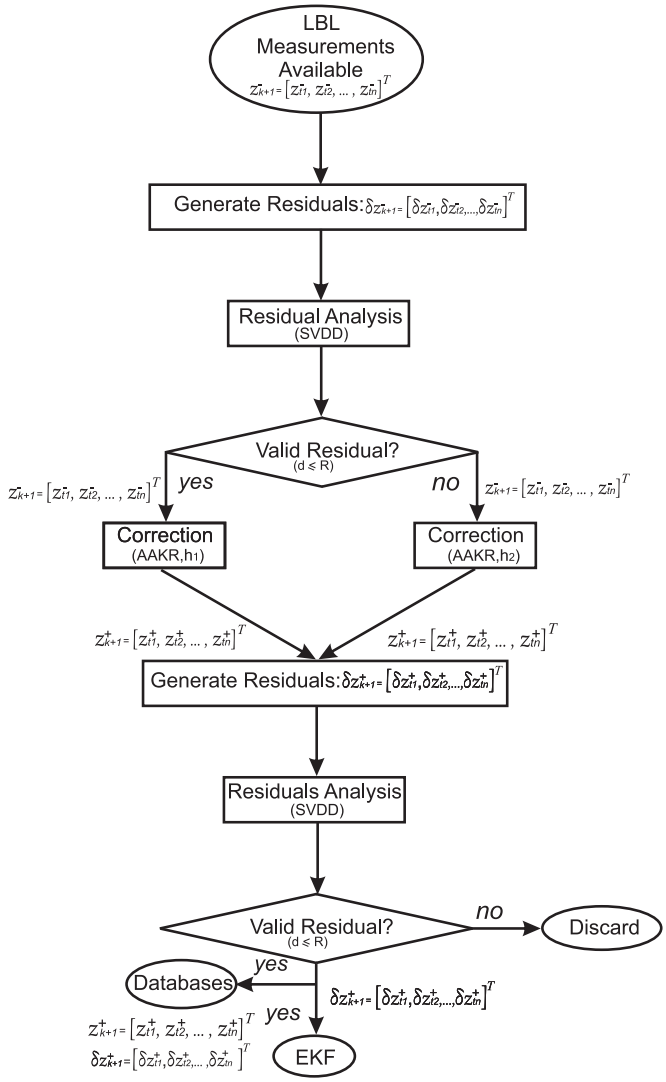

Fig. 6. Acoustic localization estimation routine. The processes of the generation of residuals, analysis of residuals, and correction and reanalysis of residuals are detailed along with the strategies adopted in each step. The kernel bandwidths h_1 and h_2 are chosen depending on the results of the acceptance test.

with a variety of ToF data acquired with a light autonomous underwater vehicle (LAUV) [43], developed in LSTS at the Faculty of Engineering, University of Porto, during missions in the port area of Leixões in Porto, Portugal. The environmental conditions were favorable to AUV navigation, with an average air temperature of 20 °C–25 °C, no rain and light winds. Moreover, the navigation area is separated from the open sea by rocks, where small boats are moored, and the water surface has small ripples with a light water current. The LBL system is deployed with two transponders or beacons (Teledyne Benthos UAT-376) at known positions, and the vehicle is equipped with a Neptune T257 transducer and a high-quality inertial measurement unit (Honeywell HG-1700). The transponders reply to the interrogations from the vehicle simultaneously, using different frequencies so that the vehicle can differentiate each one. The sound speed is estimated by an RBR XR620 conductivity–temperature–depth (CTD) sensor installed in the vehicle. In these missions, the vehicle navigates in regions of

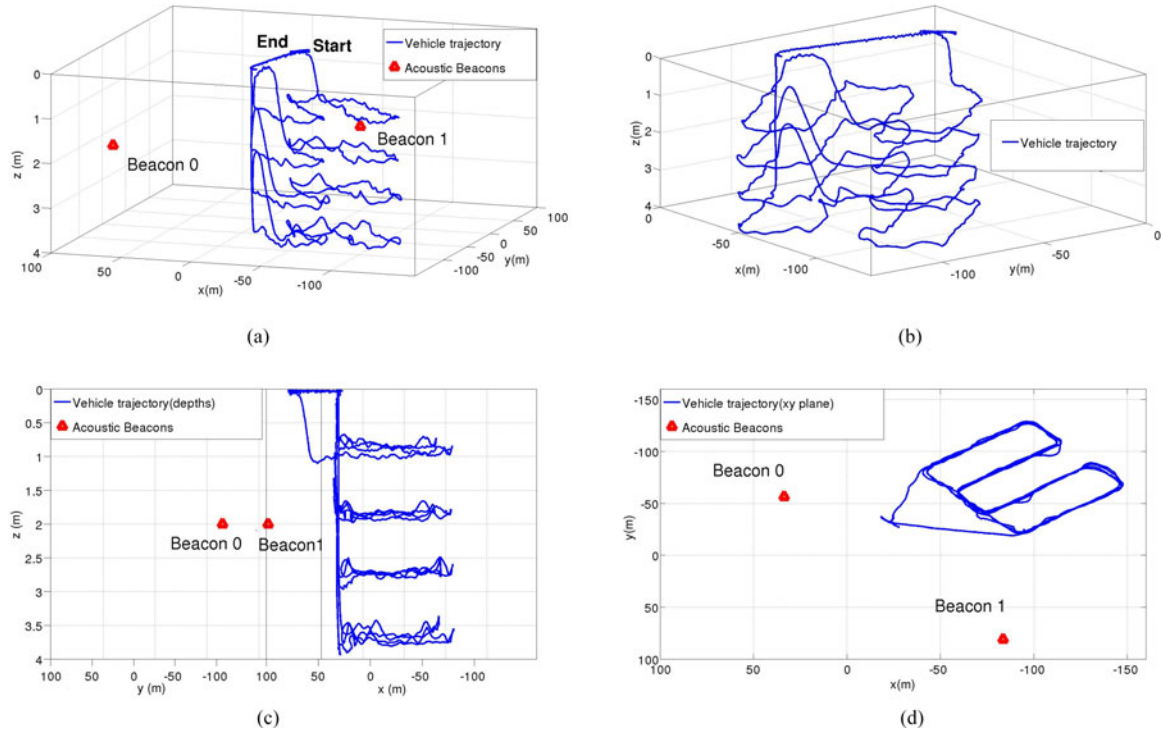

Fig. 7. Vehicle trajectory used for database composition with ToF measurements from two acoustic beacons. (a) Vehicle trajectory. (b) Vehicle trajectory (zoomed). (c) Vehicle trajectory (depths). (d) Vehicle trajectory (xy plane).

shallow water where the depth is approximately 10 m and the distance is not greater than 200 m to any of the transponders.

In the sequence, we use a set of measurements gathered from a successful mission to construct the empirical models discussed so far. It is important to emphasize that all ToF measurements, as well as the estimated quantities of them, were made excluding the coordinate z or the depth of the vehicle, which was assumed to be known from the pressure sensor. Thus, we have a greater number of measurements available at each point in the xy-plane that can be used in the correction algorithm.

A. Data Collection

The vehicle trajectory used to collect the ToF measurements that comprise the database is shown in Fig. 7. The course lasted about one and a half hours with the vehicle developing an average speed of 1.2 m/s. For the acoustic localization, the LAUV currently uses the outlier rejection scheme proposed in [44]. In this approach, the Mahalanobis distance $f(\delta z) = \delta z^T \Sigma^{-1} \delta z$ is calculated using the ToF residuals δz and its covariance matrix Σ defined from sample estimates. The result has to be smaller than a reference value $\rho = 4.0$ for a particular ToF measurement z to be considered acceptable. Analytically, we have the following classifier based on the assumption of a Gaussian distribution for the target class:

$$f(\delta z) = \begin{cases} z \text{ is target, if } & f(\delta z) \leq \rho; \\ z \text{ is outlier if } & f(\delta z) > \rho; \end{cases}$$

where the value ρ is defined empirically.

The vehicle was programmed to execute a lawnmower pattern trajectory while visiting four different depths with variation of 1 m beneath the water's surface. Regarding performance, the onboard LBL system provided the following results:

1) the total number of measurements: 721;
2) the total number of accepted measurements: 709 (beacon 0) and 708 (beacon 1);
3) the total number of rejected measurements: 12 (beacon 0); 13 (beacon 1).

As seen, due to favorable navigation conditions at the experimental site, few rejections occurred in an area of reasonable coverage and at different depths. Considering the conditions of the experiment, these outliers may come at times from the shadowing of the transducer caused by the vehicle movement, from the differences between the range-dependent water column sound-speed profile and the value measured locally by the vehicle, or from the local noise. However, there is insufficient information to prove such a claim. All data will be used in what follows to guide the choice of parameters in the correction and residual analysis algorithms.

B. Empirical Models

The process of constructing the empirical models refers to procedures adopted to set the parameters used in both algorithms, AAKR and SVDD. Thus, the previous data are used to adjust quantities such as width s in the Gaussian kernel and parameter Ω, both used in SVDD. For AAKR, the width h in the Gaussian kernel will be tuned.

1) SVDD: A very enlightening discussion is presented about the relation between parameter Ω and s in the SVDD algorithm with the Gaussian kernel in [32]. Parameter Ω controls the tradeoff between the volume and the errors in the target

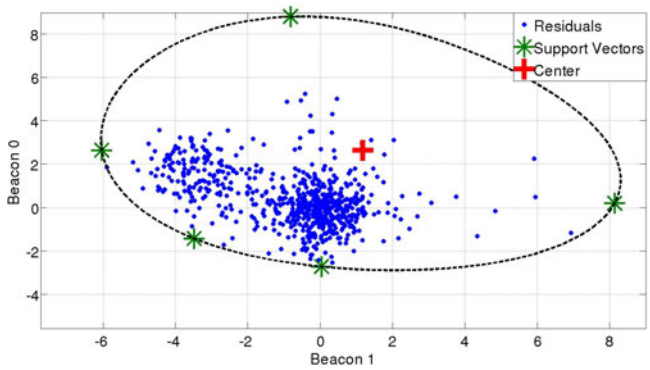

Fig. 8. Data description with residuals (m) from beacon 0 and beacon 1 measurements. SVDD kernel is a Gaussian function with width parameter s = 10 and $\Omega = 1$.

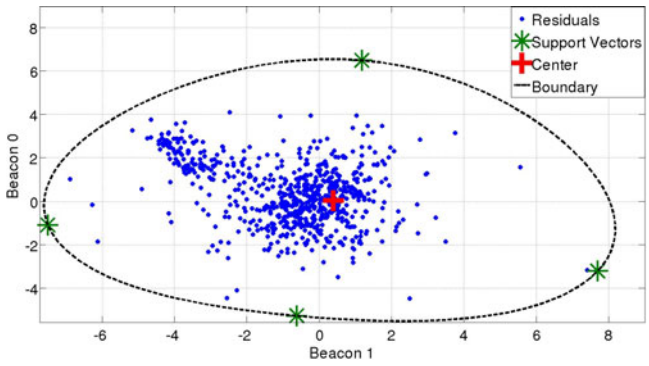

Fig. 9. Data description with residuals (m) from the AAKR output in the LOO algorithm. SVDD kernel is a Gaussian function with width parameter $s = 10$ and $\Omega = 1$.

class. Basically, when Ω decreases, the volume of data description decreases and so does the classification error in the target class. When no errors are expected in the training set, Ω can be set to 1.0, indicating that all target examples should be accepted. In this particular analysis, where the referred mission is the only source of data, parameter Ω is set to 1.0.

Regarding the width parameter s of the Gaussian kernel, it can be optimized on the basis of the required target acceptance rate. So, large s implies that the most separate examples become SV, along with a decrease in the expected error in the target class. With the available data, a well-defined region is achieved with $s \geq 5$ by using the incremental/decremental algorithm proposed in [45] to provide a fast convergence to the final solution. The next step is to run the algorithm and make fine adjustments, if necessary, to achieve a performance similar to that obtained in the original navigation. We start by choosing a small amount (≈ 20) of the total number of residuals to define the boundary region (center and radius) before execution. However, as new measurements are accepted, they are incorporated into the database to define a new boundary region for the next analysis. Fig. 8 illustrates how the accepted pairs of residuals from beacon 0 and beacon 1 are arranged in the boundary region and highlights the SVs.

The characteristics of the boundary shown in Fig. 8 are as follows:

1) radius $R = 0.70$;
2) center $a = (1.18, 2.63)$;
3) average distance to the center of the boundary region for accepted objects $\overline{d} = 0.58$;
4) average distance to the center of the boundary region for rejected objects $\overline{d} = 1.23$.

The system performance with the SVDD algorithm in the outlier rejection scheme was very similar to that obtained with the solution currently available in the vehicle:

1) the total number of accepted measurements: 715;
2) the total number of rejected measurements: 6;

2) AAKR: Considering the analysis of using the empirical model for correction, the accepted ToFs in a database are the useful information required. As mentioned, the AAKR is the strategy used here to correct deviations based on past measurements. The most important parameter in this case is width h, which controls the accuracy and the generalization capacity of the model in the regression process. In general, parameter h is found on an empirical basis using the LOO cross-validation algorithm presented in Section II-E. After running the algorithm, the cross validation, with all accepted measurements from the mission in Fig. 7, resulted in an RMSE of 0.85 m with the AAKR kernel bandwidth of 0.01.

TABLE I
PERFORMANCE WITH AND WITHOUT AAKR APPLICATION TO REJECTED VALUES

Source of Data	RMSE (m)
Raw Data	10.0
AAKR, $h = 0.01$	6.0
AAKR, $h = 1.0$	3.0

3) AAKR/SVDD: Accepted Measurements: In Fig. 9, it is interesting to visualize the change in the boundary region of the data descriptor when residuals depicted in Fig. 8, generated from accepted measurements that passed through LOO algorithm, are used in the SVDD algorithm all at once. The characteristics of the new boundary are as follows:

1) radius $R = 0.73$;
2) center $a = (0.39, 0.021)$;
3) average distance to the center of the boundary region for accepted objects $\overline{d} = 0.57$;
4) average distance to the center of the boundary region for rejected objects $\overline{d} = 1.21$.

It can be noted in the figure that the data arrangement becomes more concentrated around the center, which is now closer to point (0, 0). As parameter $\Omega = 1$, we force all accepted data to remain inside the boundary region.

4) AAKR/SVDD: Outliers Analysis: The last analysis is about the application of AAKR when the outliers observed in the mission are not rejected, and therefore, are used in EKF. This step aims to investigate the influence of the choice of kernel bandwidth on estimating measurements that were classified as unaccepted during the mission. In this analysis, all accepted measurements were used as database input so as to improve the accuracy of the measurements.

Table I summarizes the RMSE of the range in the xy-plane between the vehicle estimated position for the navigation depicted in Fig. 7, when the SVDD is used as the outlier rejection

scheme, and the estimated position, when no outlier rejection scheme is used. The analysis was carried out in two situations: 1) when the rejected measurements do not pass through the correction (raw data); and 2) when the rejected measurements pass through the correction using AAKR with different kernel bandwidths h. Given that the outlier is not represented well in the database composed with acceptable measurements, it is expected that better corrections occur with larger values of h, to weigh all available measurements.

The relation between the kernel bandwidth and the corresponding RMSE shown in Table I suggests what was previously stated about the improvements in the generalization capabilities of the AAKR for objects poorly represented by the database. In this analysis, the bandwidth was increased from 0.01 to 1.0. When small values of h are used, only examples in the database closed to the incoming data receive high weight while large values of h make the algorithm give relevant weight to all examples in the database. In this case, the output becomes a weighted average of all available examples.

V. Performance Analysis of the Proposed Design

In Section IV, both SVDD and AAKR algorithms were investigated separately to provide useful information regarding their performance when changes are made in their parameters. The SVDD confirms its capacity to fulfill the role of identifying outliers with a performance similar to the current algorithm running in the vehicle. Regarding the AAKR, the last results show how the vehicle position estimation performance is affected by changes in the kernel bandwidth, especially when we attempt to incorporate outliers. In the following sections, a new trajectory will be used to perform the analysis of the proposed complete scheme, which is shown in Fig. 1. Again, the vehicle developed an average speed of 1.2 m/s and the course lasted about 1 h. Some initial measurements are used to compose the database and construct the empirical models. After that, as navigation proceeds, these models are continuously updated.

A. Vehicle Trajectory

The vehicle trajectory for this second analysis is shown in Fig. 10. The beacons were installed close to the positions shown in Fig. 8. The regions of navigations are the same, and the environmental conditions are very similar in both missions. Regarding performance, the LBL system provided the following results:

1) the total number of measurements: 907;
2) the total number of accepted measurements: 894 (beacon 0) and 881 (beacon 1);
3) the total number of rejected measurements: 13 (beacon 0) and 26 (beacon 1).

The trajectory that was held provided a large number of ToF measurements, and both visual observation and GPS reading confirmed that the vehicle ended its mission close to the desired final endpoint, which is the location chosen before the beginning of the journey.

B. ToFs With Multipaths

To perform a useful analysis of the performance of the proposed solution, we introduce an exogenous source of errors to degrade the ToF measurements using the ray-tracing propagation model.

1) Model of Propagation: The propagation model used in this study is an extension of the scheme presented in [46] as well as the formulation used for probabilities of events. Fig. 11 shows three possible paths, besides the direct path, used for performance evaluation. The parameters are the transponder depth $H(m)$, the relative depth between the vehicle and the transponder $\Delta d(m)$, the region depth $Z(m)$, and the range in the xy-plane between the vehicle's position and the transponder $\Delta r(m)$. All variables are detailed in Fig. 11.

Based on this model, one can assume that in the propagation of sound waves, three hypotheses (Y) have a probability (P) of occurrence at instant k: direct path (DP), multiple paths (MP), and outliers (OL). In all three cases, the arrival time z_k for each emitter is modeled by the following relations:

$$z_k[i,j] = \begin{cases} \frac{1}{c}\|B_j - p(t_k)\|, & Y_k = \text{DP} \\ f_{\text{mp}}\big(p(t_k), B_j\big), & Y_k = \text{MP} \\ n_{\text{ol}}, & Y_k = \text{OL} \end{cases} \tag{31}$$

where $n_{\text{ol}} \sim \text{uniform}$.

In (31), B is the transponder position, p is the current vehicle position, and c refers to the underwater sound speed. Due to the shallow region and small ranges between the vehicle and transponders, the sound-speed profile can be considered constant throughout the water column, which simplifies the expressions. Then, the distance traveled by the sound wave in the ray tracing 1 (d_{MP_1}) can be calculated by

$$d_{MP_1} = \frac{\Delta r}{\sin(\theta)}$$
$$\theta = \arctan\left(\frac{\Delta r}{2H - \Delta d}\right). \tag{32}$$

A similar expression can be easily found for the distance traveled by the sound wave in the ray tracing 2 (d_{MP_2}). For the ray tracing 3, the distance is expressed by

$$d_{\text{MP}_3} = \frac{\Delta r}{\sin(\alpha)}$$
$$\alpha = \arctan\left(\frac{\Delta r}{2Z - \Delta d}\right). \tag{33}$$

The idea to be exploited in the validation step is to establish a probability of occurrence for each hypothesis and then replace the real measurements, under the assumption that they are obtained via the direct path, with quantities assumed obtained via multipaths or outliers within a range of $\pm$ 10 m. For purposes of comparison, considering a multipath propagation, the error is about 1.5 m per 100 m in distance.

It is also important to emphasize that all transponders were assumed to be operating in normal conditions at a fixed position as were all sensors installed in the vehicle. Thus, all accepted measurements in the mission shown in Fig. 10 were considered to be obtained from the direct path with no considerable deviations. At the occurrence of a multipath, one of the three

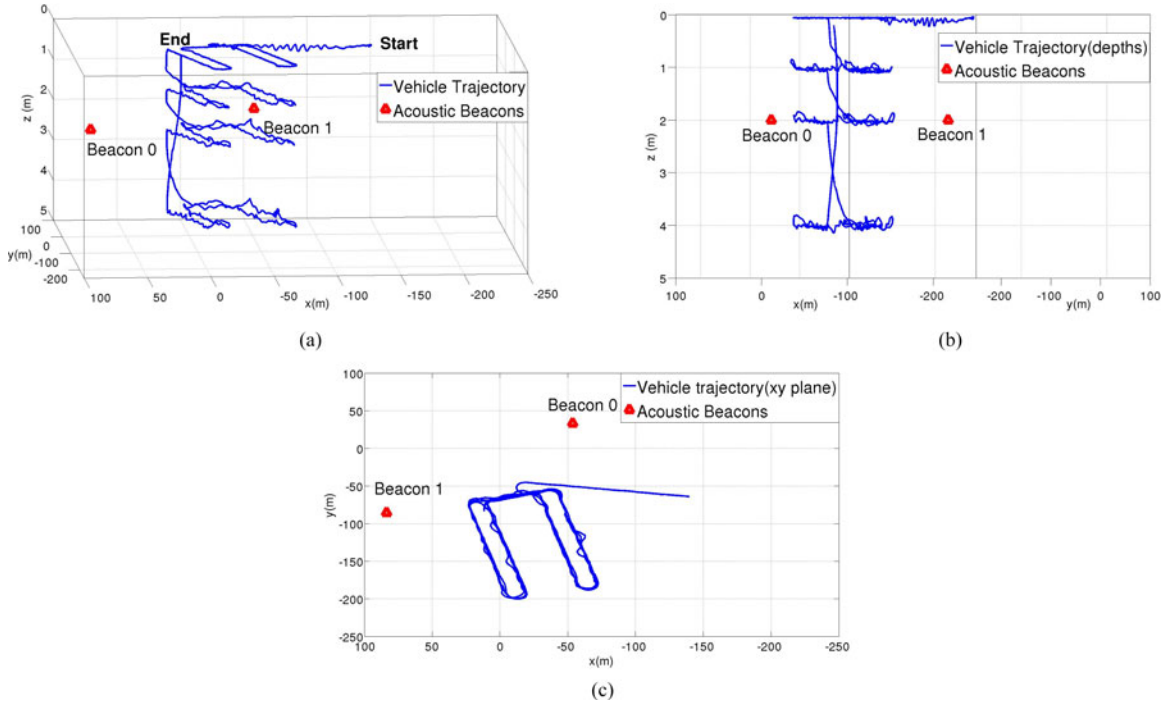

Fig. 10. Vehicle trajectory used for validation with ToF measurements from two acoustic beacons. (a) Vehicle trajectory. (b) Vehicle trajectory (depths). (c) Vehicle trajectory (xy-plane).

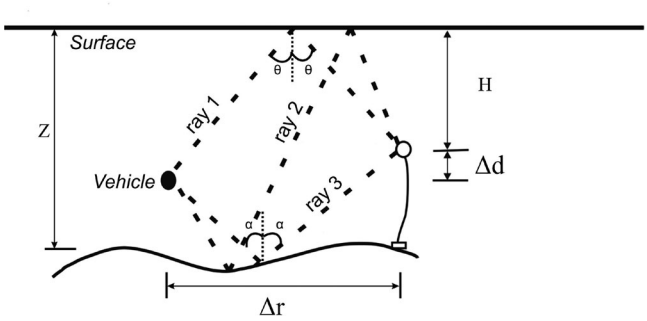

Fig. 11. Ray-tracing propagation model. Three possible paths for acoustic waves besides the direct path used for performance evaluation.

rays in Fig. 11 would be used to add such deviation to the real ToF. Fig. 12 illustrates an example of how the vehicle trajectory would be estimated due to presence of multipaths with 50% probability for propagation in the direct path. In this case, the vehicle was using its current outlier rejection scheme, and some ToF measurements from reflected waves were considered as accepted.

The result shows that, when using the propagation model presented in Fig. 11, the path followed by the vehicle shows a slight deviation of the original trajectory with a RMSE on the order of 5–15 m.

C. Metrics of Performance

The proposed scheme shown in Fig. 1 is supposed to reduce the error in the estimation of the vehicle position when the ToFs are determined from waves propagating in a multipath. The real vehicle position is supposed to be the estimated position shown in Fig. 10, and the performance of the acoustic localization estimation block is analyzed by the root mean squared error (RMSE) of the range in the xy-plane. The RMSE will be calculated by comparing the position estimation vector from the original navigation, taken as the real position, with the estimations using our strategy for acoustic localization when the model of propagation is used. Besides this quantity, the mean error in xy position will be shown to accompany the estimation behavior throughout. Section V-D is dedicated to discussing the numerical results accounting for what was discovered so far.

D. Numerical Results

In this section, the hypothesis of the propagation of rays presented in Section V-B1 takes place during vehicle navigation, and the proposed design is set to run in two parts. First, only the outlier rejection scheme with SVDD is evaluated. Then, in the second part, the performance of the whole system is analyzed.

As the first step, we have to define the probabilities for each hypothesis Y_k happening. The following configuration was assumed:

1) $Y_k = \text{DP}$: 30%;
2) $Y_k = \text{MP}$: 20% to each ray (1, 2, and 3);
3) $Y_k = \text{OL}$: 10%.

The historical measurements for AAKR database composition were gathered from the past mission depicted in Fig. 13, which was conducted near the area of navigation shown in Fig. 10.

Using the measurements from this mission, we could compose a database with 260 accepted ToF measurements before starting current navigation.

In the next analysis, the navigation system makes use of the whole algorithm in Fig. 6 where the SVDD is used for outlier rejection, whereas AAKR is used for corrections of measurement

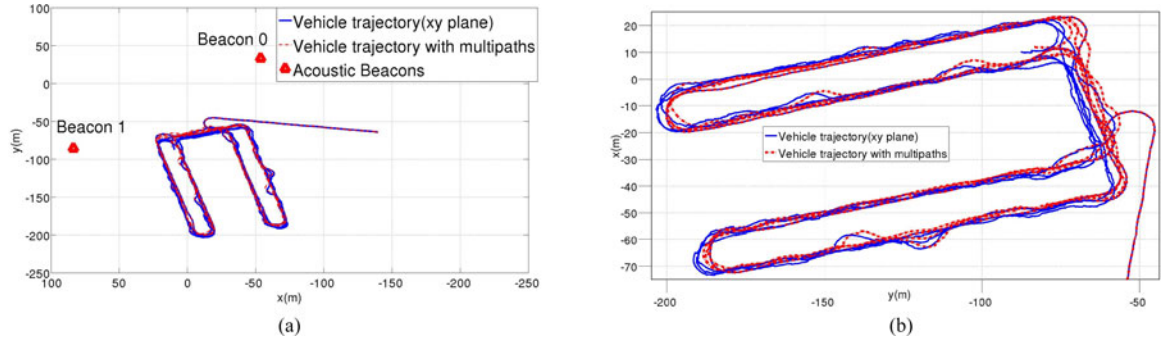

Fig. 12. Vehicle trajectories for validation. The probability for propagation in the direct path is 50%. (a) Estimated vehicle trajectory in occurrence of multipaths. (b) Estimated vehicle trajectory in occurrence of multipaths (zoomed).

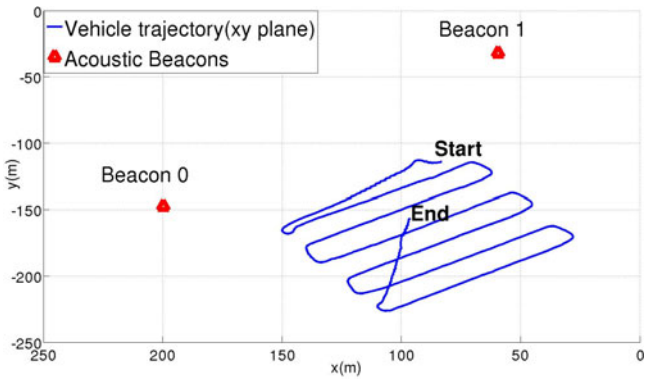

Fig. 13. Vehicle trajectory for database composition. Mission accomplished on a different day of previous missions shown.

TABLE II
KERNEL BANDWIDTH ADJUSTMENT BASED ON RESIDUAL ANALYSIS

Distance to the Center of the Hypersphere (d)	Kernel Bandwidth (h)
$d \leq R$	$h = 0.01$
$R < d \leq 1.5R$	$h = 0.05$
$1.5R < d \leq 2R$	$h = 0.1$
$2R < d$	$h = 1.0$

deviations. The measurements gathered from the mission depicted in Fig. 13 were initially used to perform corrections to the coming ToFs, and the residuals were used to define a boundary region for data classification, which, at this time, provides useful information for the correction algorithm so that it can choose the kernel bandwidth according to the rule shown in Table II.

The values of the kernel bandwidth h were chosen after several simulations to obtain the best results, taking into account the distance that the residual is located at from the center of the hypersphere and the tuning procedure discussed in Sections IV–B2 and IV-B4. The idea here is to adapt the AAKR algorithm for measurements that generated residuals that were poorly represented by the database. To exploit the flexibility of the proposed solution, we decided to increase the tolerance for acceptance of measurements by setting the kernel parameter at a large value $(s = 20)$. However, to limit the hypersphere coverage, we assume the presence of outliers in the training database and then set parameter $\Omega < 1$ for reasons discussed in Section II-D. The assumption of the presence of outliers in the training set will force the algorithm to keep the more likely sort of data inside the hypersphere.

TABLE III
RMSE WITH THE PROPOSED ACOUSTIC LOCALIZATION ESTIMATION

Algorithm	RMSE (m)				
No outlier rejection algorithm	7.3	8.2	8.6	8.8	10.0
Current onboard outlier rejection algorithm	1.93	2.10	2.16	2.42	2.58
SVDD/AAKR aided navigation	1.30	1.31	1.68	1.15	1.41

Table III shows a comparison of the localization system performance when the proposed approach replaces the current onboard outlier rejection algorithm. The errors are clearly reduced when the combination of algorithms for correction (AAKR) and for classification (SVDD) are used. Again, the presented metric is the RMSE of the range in the xy-plane between the original vehicle trajectory and the estimated one when exogenous synthetic errors are inserted.

It is important to emphasize that the comparative results shown in Table III between the two approaches are directly related to the assumed values for the probabilities of occurrence of ray propagation by the direct path, multiple paths, and outliers. Situations where the occurrence of ray propagation by multiple paths or outliers is low led to similar performance for both strategies. On the other hand, an excessive occurrence of incorrect measurements makes both solutions unable to judge the validity of such data and the vehicle loses its orientation completely. However, what the results testify about the proposed architecture is its ability to learn to classify the measurements based on historical data with the relevant role of the correction algorithm to sustain an accurate judgment during navigation.

Fig. 14 shows the mean error in the xy positions for the case previously mentioned. The result behaves as expected once the outlier rejection scheme avoids large deviation from the real trajectory. The proposed solution was capable of reducing the error between the real and estimated positions of the vehicle.

The large error in the first part of the mission seen in Fig. 14 is related to the beginning of the navigation, which is always a difficult period for navigation because the vehicle is too close to the water's surface. Moreover, at the start, the vehicle performs various calibration procedures, including adjusting the speed of sound in water. All these aspects result in a large number of outliers being accepted or, in the case of discarding measurements,

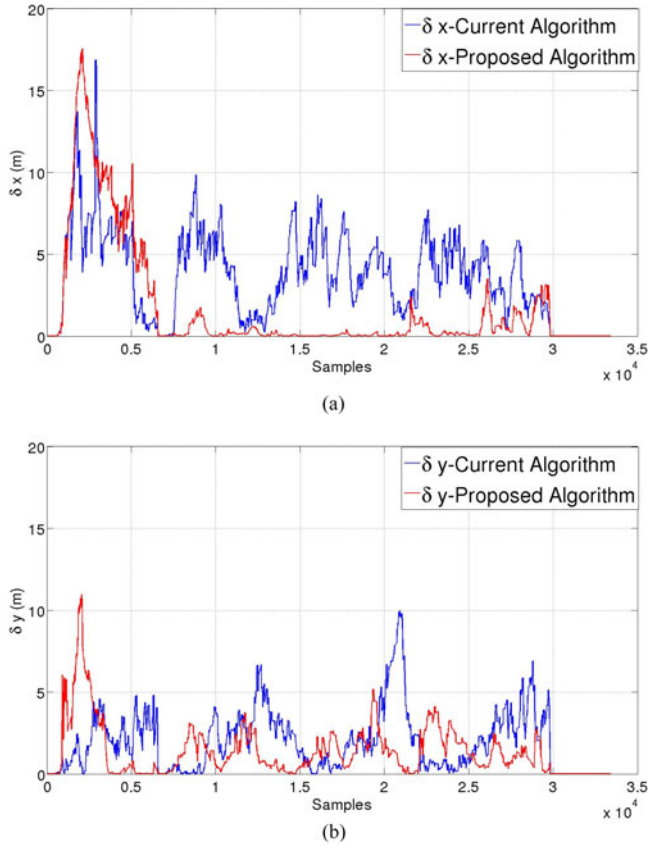

Fig. 14. The mean error in xy positions of both strategies for underwater acoustic localization. (a) The mean error in x position (δx). The mean error in y position (δy).

make the vehicle navigate a long time without any correction from the LBL system.

Regarding the proposed solution, the AAKR failed to make significant corrections to improve the accuracy of the navigation because initially the algorithm had only measurements from other missions, which may not be satisfactory. As navigation proceeds, we can discard the database with measurements from other missions and use values obtained on the spot.

An example of the hypersphere obtained in this analysis that considered the presence of outliers in the training set is shown in Fig. 15. It is possible to identify some examples from the training set that stayed outside the boundary region. These examples correspond to SVs with $\alpha_i = \Omega$ from (25) and, along with those residuals on the boundary, define the data descriptor.

It is worth remarking that in all cases analyzed, the real position of the vehicle is actually unknown, and all measurements from previous missions that were considered valid to compose the database could have some unavoidable deviations.

VI. Analysis and Comments

In view of what has been discussed so far, some topics in the proposed solution should be emphasized to be exploited afterward. First, the proposed solution provides flexibility regarding the choices of its parameters aiming for better adaptation to the navigation environment.

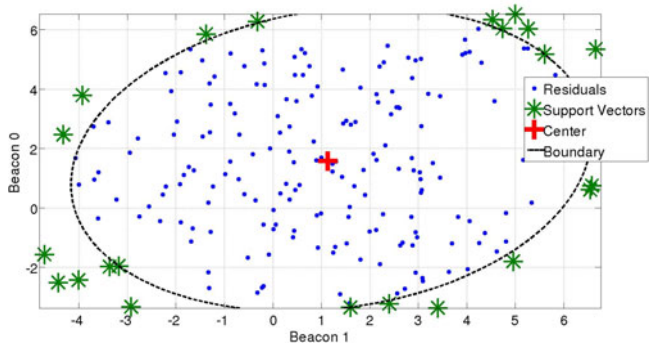

Fig. 15. Data description with residuals (m) from beacon 0 and beacon 1 measurements. SVDD kernel is a Gaussian function with kernel width parameter $s = 20$ and with the assumption of a percentage of outliers in the target set $\Omega = 0.2$. Examples outside and on the boundary are SVs that define the data descriptor.

1) Optimize parameter Ω for both negative and positive examples once it reflects the percentage of negative examples in the target and outlier set [32].
2) Increase the feature dimension to improve the data description.
3) Establish a rule to remove elements in the target set as its distance to the center of the hypersphere increases with time.
4) Weigh each ToF measurement differently according to its distance to the center of the hypersphere so they can be used in other regression functions by using SVMs [47], for instance, or directly in EKF by giving more relevance to some measurement than others.

However, troublesome issues in the solution need to be highlighted. One of the limitations comes from the poor extrapolation of AAKR, which presents satisfactory results when recent measurements are made in the navigation area and when the query data are well represented in the model. Nevertheless, by using ToF only in the xy-plane, we could have more measurements available in the correction process associated to each position. Still regarding the AAKR, the algorithm must be well tuned with respect to its parameters to return satisfactory results. Moreover, in our analysis, all measurements that are considered accepted and used for correction were gathered on the basis of estimated vehicle position during its navigation, but a set of training data collected from the vehicle position determined by a global positioning system would make the presented analysis more accurate.

Regarding the SVDD, the usage of residuals for one-class classification also requires a careful choice of samples for data description due to rapid changes in the stochastic properties of the acoustic channel. Thus, the usage of all target examples from past missions is quite difficult, but it was exploited here to show some possibilities of the proposed solution.

As stated in the work, the SV data description basically finds the smallest hypersphere around the target class but it requires a difficult optimization. However, many solutions have been proposed to perform online optimization processes as new data arrive [45], [48], [49], i.e., incrementally, which reduces the computational cost. Regarding the execution time, by using a 2.1-GHz processor, our algorithm took from a few milliseconds,

for a small training set, to 50–80 ms, for a large amount of data, to find the center and the radius of the hypersphere when a new ToF measurement became available. An important aspect that limits the analysis of the proposed solution is the use of only two acoustic beacons in our experiment and the processing of only ToF information. We expect that, when more correlated information is extracted from the acoustic signal coming from various acoustic beacons, more accurate the classification of measurements will be. It is an open area of research and certainly deserves further investigation.

VII. Conclusion

The underwater navigation system in environments that exhibit unpredictable behavior regarding changes in noise statistics and dynamics requires a certain level of adaptability in the measurement system, mainly for acoustic sensing. Manufacturers of acoustic equipment emphasize the importance of calibration in LBL systems to identify underwater channel characteristics, such as the temperature and sound-speed profiles. The EKF, aided by external sensors, is made sufficiently robust to short oscillations in the acoustic sensing quality, but can be degraded by continuous deviations. To deal with these issues, this paper exploits algorithms based on historical measurements for underwater acoustic localization using LBL configuration. The proposed algorithm takes advantage of more accurate measurements to make better decisions about the acceptance and estimation of ToF measurements.

An SVDD looks at the generated residuals to keep similar examples inside a boundary region and to detect outliers. It should be noted that no assumption about the statistics of the data was made, leaving the system to record the behavioral data as navigation proceeds. At the same time, an AAKR function makes corrections in the ToFs measurements based on previous measurements. The interaction between both algorithms results in a better description of the data and a better ability to correct deviations.

The presented design seems to be very appropriate for low-cost vehicles once it provides a good solution without computation overload and can also be attached to any data fusion algorithm for navigation. With the use of real data, the proposed localization system is validated, and some of its potentialities are investigated. As a future work, we recommend the implementation of the algorithm on a vehicle and its validation in the field.

Acknowledgment

The authors would like to thank Programa de Ciência, Tecnologia e Inovação—PTI C&T + I from Fundação Parque Tecnológico Itaipu—Brasil, FPTI-BR and Programa CAPES/FCT/BEX-7828/12-8 of international cooperation—Brasil/Portugal.

References

[1] L. M. M. Dunbabin, "Robotics for environmental monitoring," *IEEE Robot. Autom. Mag.*, vol. 19, no. 1, pp. 24–39, Mar. 2012.

[2] M. Jacobi and D. Karimanzira, "Underwater pipeline and cable inspection using autonomous underwater vehicles," in *Proc. MTS/IEEE OCEANS Conf.*, 2013, DOI: 10.1109/OCEANS-Bergen.2013.6608089.

[3] B. Hobson, *et al.*, "Tethys-class long range AUVs—extending the endurance of propeller-driven cruising AUVs from days to weeks," in *Proc. IEEE/OES Autonom. Underwater Veh.*, Sep. 2012, DOI: 10.1109/AUV.2012.6380735.

[4] M. Furlong, *et al.*, "Autosub long range: A long range deep diving AUV for ocean monitoring," in *Proc. IEEE/OES Autonom. Underwater Veh.*, Sep. 2012, DOI: 10.1109/AUV.2012.6380737.

[5] D. Thompson, *et al.*, "MBARI mapping AUV operations: In the Gulf of California," in *Proc. OCEANS Conf.*, Oct. 2012, pp. 1–5.

[6] A. Alcocer, P. Oliveira, and A. Pascoal, "Underwater acoustic positioning systems based on buoys with GPS," in *Proc. 8th Eur. Conf. Underwater Acoust.*, Carvoeiro, Portugal, 2006.

[7] A. Caiti, V. Calabro, T. Fabbri, D. Fenucci, and A. Munafo, "Underwater communication and distributed localization of AUV teams," in *Proc. MTS/IEEE OCEANS Conf.*, 2013, DOI: 10.1109/OCEANS-Bergen.2013.6608166.

[8] P. A. Miller, J. A. Farrell, and V. Y. Z. Djapic, "Autonomous underwater vehicle navigation," *IEEE J. Ocean. Eng.*, vol. 35, no. 3, pp. 663–678, Jul. 2010.

[9] A. Caiti, A. Garulli, F. Livide, and D. Prattichizzo, "Localization of autonomous underwater vehicles by floating acoustic buoys: A set-membership approach," *IEEE J. Ocean. Eng.*, vol. 30, no. 1, pp. 140–152, Jan. 2005.

[10] G. Donovan, "Position error correction for an autonomous underwater vehicle inertial navigation system (INS) using a particle filter," *IEEE J. Ocean. Eng.*, vol. 37, no. 3, pp. 431–445, 2012.

[11] K. Vickery, "Acoustic positioning systems. New concepts—The future," in *Proc. 1998 Workshop Autonom. Underwater Veh.*, Aug. 1998, pp. 103–110.

[12] P. Milne, *Underwater acoustic positioning systems*, Gulf Pub. Co., 1983.

[13] A. Apartsin, L. Cooper, and N. Intrator, "Semi-coherent time of arrival estimation using regression," *J. Acoust. Soc. Amer.*, vol. 132, no. 2, pp. 832–837, 2012.

[14] K.-C. Lee, J.-S. Ou, and L.-T. Wang, "Underwater acoustic localization by probabilistic fingerprinting in eigenspace," in *Proc. MTS/IEEE OCEANS Conf., Marine Technology for Our Future: Global and Local Challenges*, 2009, pp. 1–4.

[15] K.-C. Lee, J.-S. Ou, and M.-C. Huang, "Underwater acoustic localization by principal components analyses based probabilistic approach," *Appl. Acoust.*, vol. 70, no. 9, pp. 1168–1174, 2009.

[16] K.-C. Lee, J.-S. Ou, M.-C. Huang, and M.-C. Fang, "A novel location estimation based on pattern matching algorithm in underwater environments," *Appl. Acoust.*, vol. 70, no. 3, pp. 479–483, 2009.

[17] V. Vapnik, "An overview of statistical learning theory," *IEEE Trans. Neural Netw.*, vol. 10, no. 5, pp. 988–999, 1999.

[18] H.-J. Wang, J. Wang, L. Yu, and Z.-Y. Liu, "A new SLAM method based on SVM-AEKF for AUV," in *Proc. OCEANS Conf.*, 2011, pp. 1–6.

[19] M. Martnez-Ramón, N. Xu, and C. Christodoulou, "Antenna array processing for radar applications with support vector machines," in *Ultra-Wideband Short-Pulse Electromagnetics 8*, C. Baum, A. Stone, and J. Tyo, Eds., New York, NY, USA: Springer-Verlag , 2007, pp. 143–151.

[20] C. Christodoulou and M. M. Ramon, *Support Vector Machines for Antenna Array Processing and Electromagnetics*, 1st ed., ser. Lectures on Computational Electromagnetics, C. Balanis, Ed., London, U.K.: Morgan & Claypool, Oct, 2006.

[21] B. Pinheiro, U. Moreno, J. de Sousa, and O. Rodriguez, "Improvements in the estimated time of flight of acoustic signals for AUV localization," in *Proc. MTS/IEEE OCEANS Conf.*, 2013, DOI: 10.1109/OCEANS-Bergen.2013.6608178.

[22] T. I. Fossen, *Guidance and Control of Ocean Vehicles*, London, U.K.: Wiley, 1994.

[23] K. R. Britting, *Inertial Navigation Systems Analysis*, Norwood, MA, USA: Artech House, 2010.

[24] P. M. Lee, *et al.*, "Simulation of an inertial acoustic navigation system with range aiding for an autonomous underwater vehicle," *IEEE J. Ocean. Eng.*, vol. 32, pp. 327–345, Apr. 2007.

[25] M. Morgado, P. Oliveira, C. Silvestre, and J. Vasconcelos, "USBL/INS tightly-coupled integration technique for underwater vehicles," in *Proc. 9th Int. Conf. Inf. Fusion*, Jul. 2006, DOI: 10.1109/ICIF.2006.301607.

[26] C. Moler and C. V. Loan, "Nineteen dubious ways to compute the exponential of a matrix," *SIAM Rev.*, vol. 20, pp. 801–836, 1978.

[27] H. Ramezani and G. Leus, "Ranging in an underwater medium with multiple isogradient sound speed profile layers," *Sensors*, no. 12, pp. 2996–3017, 2012.

[28] H. Medwin and C. S. Clay, *Fundamentals of Acoustical Oceanography (Applications of Modern Acoustics)*, 1st ed., New York, NY, USA: Academic, Oct. 1997.

[29] S. Appleby and J. Davies, "Time, frequency and angular dispersion modelling in the underwater communications channel," in *Proc. OCEANS Conf.*, Sep. 1998, vol. 2, pp. 644–649.
[30] M. Stojanovic and J. Preisig, "Underwater acoustic communication channels: Propagation models and statistical characterization," *IEEE Commun. Mag.*, vol. 47, no. 1, pp. 84–89, Jan. 2009.
[31] D. M. J. Tax, "One-class classification—Concept-learning in the absence of counter-examples," Ph.D. dissertation, Delft Univ. Technol., Delft, The Netherlands, 2001.
[32] D. M. J. Tax and R. P. W. Duin, "Support vector data description," *Mach. Learn.*, vol. 54, no. 1, pp. 45–66, Jan. 2004.
[33] V. N. Vapnik, *Statistical Learning Theory*, New York, NY, USA: Wiley-Interscience, 1998.
[34] V. Vapnik, "An overview of statistical learning theory," *IEEE Trans. Neural Netw.*, vol. 10, no. 5, pp. 988–999, 1999.
[35] D. M. J. Tax and R. P. W. Duin, "Support vector domain description," *Pattern Recognit. Lett.*, vol. 20, pp. 1191–1199, 1999.
[36] B. Schölkopf and A. J. Smola, *Learning with kernels: Support vector machines, regularization, optimization, and beyond*, ser. Adaptive Computation and Machine Learning, Cambridge, MA, USA: MIT Press, 2002.
[37] D. Tax, "Ddtools, the data description toolbox for matlab," Jun. 2015, version 2.1.2.
[38] E. Parzen, "On estimation of a probability density function and mode," *Ann. Math. Stat.*, vol. 33, no. 3, pp. 1065–1076, 1962.
[39] S. Girard and S. Iovle, "Auto associative models and generalized principal component analysis," Institut National de Recherche en Informatique et en Automatique, Montbonnot-St-Martin, France, Repport de Recherche 4364, Janvier 2002, Thème 4—Simulation et optimisation de systèmes complexes.
[40] D. F. Specht, "A general regression neural network," *IEEE Trans. Neural Netw.*, vol. 2, no. 6, pp. 568–576, 1991.
[41] R. Chevalier, D. Provost, and R. Seraoui, "Assessment of statistical and classification models for monitoring EDFs assets," in *Proc. 6th Amer. Nuclear Soc. Int. Top. Meeting Nuclear Plant Instrumentation, Control and Human-Machine Interface Technologies*, 2009.
[42] V. Cherkassky and F. Mulier, *Learning From Data: Concepts, Theory and Methods*, New York, NY, USA: Wiley, 1998.
[43] L. Madureira, *et al.*, "The light autonomous underwater vehicle: Evolutions and networking," in *Proc. MTS/IEEE OCEANS Conf.*, 2013, DOI: 10.1109/OCEANS-Bergen.2013.6608189.
[44] J. Vaganay, J. Leonard, and J. Bellingham, "Outlier rejection for autonomous acoustic navigation," in *Proc. IEEE Int. Conf. Robot. Autom.*, 1996, vol. 3, pp. 2174–2181.
[45] D. M. J. Tax and P. Laskov, "Online SVM learning: from classification to data description and back." in *Proc. IEEE 13th Workshop Neural Netw. Signal Process.*, 2003, pp. 499–508.
[46] B. Bingham and W. Seering, "Hypothesis grids: Improving long baseline navigation for autonomous underwater vehicles," *IEEE J. Ocean. Eng.*, vol. 31, no. 1, pp. 209–218, 2006.
[47] W. Huang and L. Shen, "Weighted support vector regression algorithm based on data description," in *Proc. ISECS Int. Colloq. Comput. Commun. Control Manage.*, 2008, vol. 1, pp. 250–254.
[48] J. Ma, J. Theiler, and S. Perkins, "Accurate online support vector regression," *Neural Comput.*, vol. 15, pp. 2683–2703, 2003.
[49] J. Kivinen, A. J. Smola, and R. C. Williamson, "Online learning with kernels," *IEEE Trans. Signal Process.*, vol. 52, no. 8, pp. 2165–2176, 2004.

Breno C. Pinheiro received the B.S. degree in electrical engineering from Federal University of Ceará, Fortaleza, Brazil, in 2004 and the M.S. and Ph.D. degrees in automation and systems engineering from Federal University of Santa Catarina, Florianópolis, Brazil, in 2009 and 2015, respectively.

Currently, he is a Professor at the Electrical Engineering Department, State University of Western of Paraná, Paraná, Brazil. His research interests are in embedded real-time control systems and unmanned vehicles.

Ubirajara F. Moreno was born in S. Bernardo do Campo, Brazil, in 1971. He graduated in industrial electrical engineering from the Federal Technological University of Paraná, Paraná, Brazil, in 1994 and received the M.S. degree in electrical engineering from the Federal University of Santa Catarina, Florianópolis, Brazil, in 1997 and the Ph.D. degree in electrical engineering from Universidade Estadual de Campinas, Campinas, Brazil, in 2001.

He is currently a Professor at the Federal University of Santa Catarina, Florianópolis, Brazil. He has experience in automation and systems, acting on the following topics: networked control systems, cooperative control, mobile robotics, monitoring systems, and engineering education.

João T. B. de Sousa has been leading the design, implementation, and deployment of advanced unmanned vehicle systems with the support of projects funded by the Portuguese Foundation for Science and Technology, the Portuguese Ministry of Defense, NATO, and the European Union, and also by ONR and DARPA in the United States. He has coauthored 20 journal papers as well as over 200 conference papers. His research interests include unmanned vehicles, control architectures, control and coordination, and dynamic optimization.

Dr. de Sousa is a member of the AUVSI maritime advisory committee. In 2006, he received the national BES Innovation National Award for the design of the light autonomous underwater vehicle. In 2007, he received an outstanding teaching award from Porto University.

Orlando C. Rodríguez received the M.Sc. degree in physics from Lomonosov State University, Moscow, Russia, in 1992 and the Ph.D. degree in geophysics from the University of Algarve (UALG), Faro, Portugal, in 2001.

Currently, he is an Assistant Professor at the Physics Department, UALG, with a broad and long experience of teaching. His research is being developed at the Signal Processing Laboratory (SiPLAB), working in the field of ocean underwater acoustics, mostly focused in 3-D modeling and ray tracing. Connected to his research he has acted as advisor of M.Sc. and Ph.D. students in Portugal and abroad. He is the author of the TRACEO Gaussian Beam model.